

# Mechanical effect of capillary forces in the crack tip of a DCDC specimen

M. Ciccotti<sup>1,\*</sup>, G. Pallares<sup>1,2</sup>, L. Ponson<sup>3</sup>, A. Grimaldi<sup>1</sup> and M. George<sup>1</sup>

<sup>1</sup> *Laboratoire des Colloïdes, Verres et Nanomatériaux, CNRS, University Montpellier 2, France*

<sup>2</sup> *CEA, IRAMIS, SPCSI, Grp. Complex Systems & Fracture, F-91191 Gif Sur Yvette, France*

<sup>3</sup> *Division of Engineering and Applied Science, California Institute of Technology, Pasadena, CA 91125, USA*

\* ciccotti@lcvn.univ-montp2.fr

**Abstract.** DCDC is widely used to study sub-critical crack propagation in brittle materials due to elevated crack propagation stability. This quality has made this test suitable for in-situ AFM observations of the neighbourhood of the crack tip at low propagation velocities. In a recent work we reported direct evidence of the presence of a submetric liquid condensate at the crack tip of a fused silica glass. The AFM phase imaging technique allows measuring the condensation length as a function of the applied stress intensity factor and relative humidity. In order to relate this length to a critical condensation distance between the opposite crack surfaces, a detailed knowledge of the crack opening is required. We realized an experimental investigation of the crack opening profile by reflection interferometry and compared the results with a 2D finite element simulation of a cracked DCDC specimen including the mechanical effect induced by the liquid condensation.

**Keywords :** DCDC - Finite Element simulations - Linear Elastic Fracture Mechanics - Capillary forces

## 1 Introduction

The Double Cleavage Drilled Compression (DCDC) sample refers to a parallelepipedic column with a circular hole drilled through its center that is subjected to axial compression. This geometry provides many advantages in studying the fracture of brittle materials. Janssen originally introduced such a fracture test for measuring the fracture toughness of glass [1]. Under a uniform axial compression, the Poisson effect produces a tensile stress concentrated around the central hole. This induces the initiation of two symmetric mode I crack generated at each crown of the hole and propagating along the mid-plane of the sample as the axial compression is increased (see Figs. 1 and 3). The high stability of the crack propagation has made of the DCDC a rather popular fracture test geometry used in various contexts ranging from studies on sub-critical crack propagation in oxide glasses [2],[3],[4],[5], on crack healing in

polymers [6] or on failure behavior under mixed mode loading for linear elastic materials [7],[8].

The present study presents a coupled theoretical and experimental investigation of the crack opening profile in the DCDC specimen. A 2D Finite Element (FE) simulation is compared with a direct measurement of the crack opening profile by monochromatic light reflection interferometry on a silica glass specimen. The results are expressed in a simple form as a function of the geometrical parameters of the specimen following a Williams expansion series and provide a solid base for the interpretation of recent experiments on the nanoscale capillary condensation of water inside sharp cracks in glass [4].

## 2 Finite Element simulation of DCDC specimens

### 2.1 Loading configuration and finite element mesh

The finite element simulation used to estimate the crack opening profile of the DCDC specimens is based on a 2D plane strain analysis implemented by the finite element code CAST3M<sup>1</sup>. The plane strain condition is chosen to model the behavior of the sample in its mid-plane, where the experimental measurements are done. The details of the sample loading configuration and the mesh geometry are shown in Fig. 1. The sample consists of a prism of dimensions  $2w \times 2t \times 2L$  with a cylindrical cross hole of radius  $R$  drilled through the specimen (thickness  $2t$ ). The sample is loaded with a compressive stress  $\sigma$  applied to the two opposite faces. The Poisson's ratio and the Young's modulus were set to  $\nu = 0.17$  and  $E = 72$  GPa respectively (to represent the properties of silica glass used for the experiments). However, let us note that the influence of  $E$  on the result of simulations is explicitly given in the following while the effect of  $\nu$  is minor (inferior to 1 % in the range  $0.1 < \nu < 0.4$ ). During the test, two symmetric cracks propagate from the central hole in opposite directions along the midplane of the sample (the length  $a$  of each crack is calculated from the side of the hole). Thanks to the symmetry of the geometry, one can limit the simulation to one quarter of the specimen (composed of about 3500 nodes), imposing specific boundary conditions to the system (cf. Fig. 1 bottom), i.e.  $u_x = 0$  along the symmetry plan normal to  $\vec{e}_x$  and  $u_y = 0$  along the one normal to  $\vec{e}_y$  on the uncracked ligament. The gap between the millimeter length scale of the external mechanical loading and the nanometric length scale of the crack opening near the tip requires an adapted mesh for the calculation of stress and displacement fields. To analyze such a multi-scale problem without overcoming reasonable computational times, the elements of the mesh are chosen so that their size decreases exponentially while approaching the crack tip, down to a minimum element size of 0.01 nm. To investigate the influence of the geometrical parameters on the crack opening

---

<sup>1</sup>CAST3M software is developed by CEA-Saclay, France. Reference web page : <http://www-cast3m.cea.fr/cast3m/index.jsp>

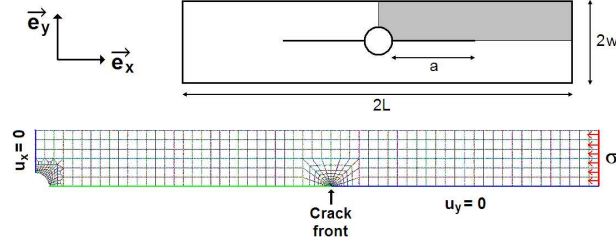


FIG. 1 – Sketch of the DCDC specimen and details of the numerical simulation : The mesh used in the finite element calculations is only one quarter of the whole sample represented in grey on the scheme of the geometry. The element size decreases exponentially when approaching the crack tip, so that deformations of the crack profile up to some nanometers from the crack tip can be computed

profile, a first series of meshes was designed with seven values for the hole radius  $R$  ranging from 0.4 mm ( $w/R = 5$ ) to 0.8 mm ( $w/R = 2.5$ ), keeping the width and length constant with  $w = 2$  mm and  $L = 20$  mm. The effect of the specimen width on the opening profile is studied using another series of seven meshes, varying  $w$  from 1 mm to 4 mm while keeping radius and length constant with  $R = 0.8$  mm and  $L = 20$  mm. For each new geometry, the crack length  $a$  was changed between 2.5 and 18.0 mm with 0.1 mm steps.

## 2.2 Crack opening profile in the absence of internal forces

In the absence of internal forces the first 2 mm of the crack opening profile (Figure 2) in our DCDC geometry is shown to be well approximated (to 1%) by the a Williams expansion [9] in the form :

$$w_y^{Ext}(X) = \frac{K_I}{E'} \sqrt{\frac{8}{\pi}} \left( X^{1/2} + \alpha_3 X^{3/2} + \alpha_5 X^{5/2} \right) \quad (1)$$

where  $\alpha_3 = 1.319/w \text{ m}^{-1}$  and  $\alpha_5 = 0.515/w \text{ m}^{-2}$  in the domain of validity ( $w \leq a \leq L - 2w$ ). The stress intensity factor  $K_I$  caused by the external loading  $\sigma$  can be expressed in adimensional form as a function of  $a/R$  and  $w/R$  according to :

$$\frac{\sigma \sqrt{\pi R}}{K_I} = \left[ c_0 + c_1 \frac{w}{R} + c_2 \left( \frac{w}{R} \right)^2 \right] + \left[ c_3 + c_4 \frac{w}{R} + c_5 \left( \frac{w}{R} \right)^2 \right] \frac{a}{R} \quad (2)$$

with the set of parameters :  $c_0 = -0.6483$ ,  $c_1 = 6.9136$ ,  $c_2 = 2.0757$ ,  $c_3 = -6.6879$ ,  $c_4 = 4.7855$ ,  $c_5 = -0.0910$ .

The 1% range of validity of the first order (corresponding to Irwin equation [10]) and the third order expansion are shown to be respectively  $\xi_1 = 20 \text{ } \mu\text{m}$  and  $\xi_3 = 300 \text{ } \mu\text{m}$ .

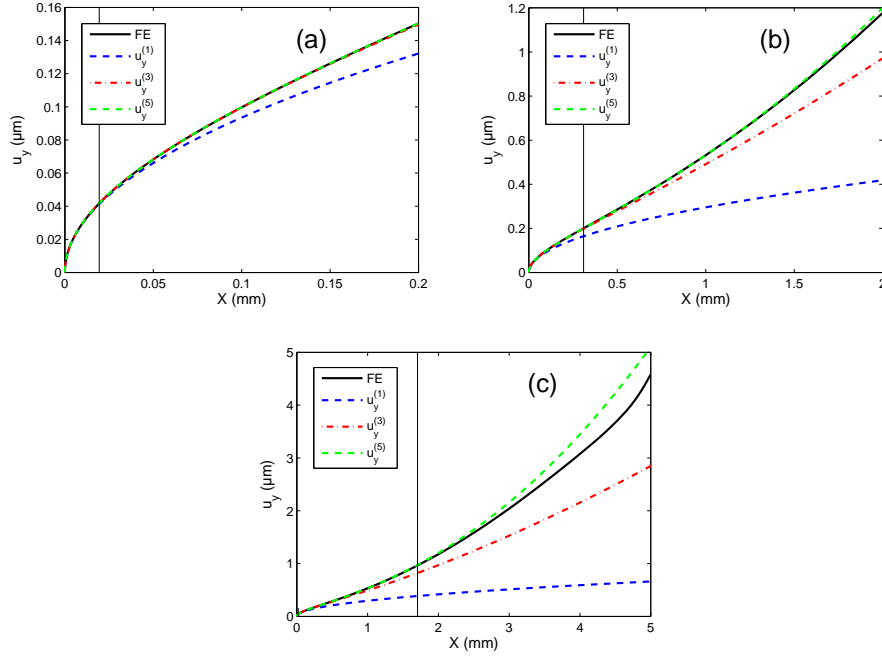


FIG. 2 – Comparison between the crack opening profile obtained by FE simulation and the Williams series of order 1, 3, and 5 at different scales : (a) at the micrometer scale ; (b) at the millimeter scale ; (c) on the whole length of the crack. The vertical lines at  $20 \mu\text{m}$ ,  $300 \mu\text{m}$  and  $1.7 \text{ mm}$  represent the 1 % limit of validity of  $u_y^{(1)}$ ,  $u_y^{(3)}$  and  $u_y^{(5)}$ , respectively

### 3 Experimental measurement by reflection interferometry

The experimental measurement of the crack opening profile is performed by using a precision loading apparatus (based on a Microtest load cell produced by Deben, Woolpit, UK) providing highly stable failure conditions necessary for in-situ observations of slow crack propagations in glasses by Atomic Force Microscopy (AFM) [11]. DCDC samples of pure silica glass (Suprasil 311, Heraeus, Germany) are machined into  $4 \times 4 \times 40 \text{ mm}^3$  rods ( $w = 2 \text{ mm}$  and  $L = 20 \text{ mm}$ ) and polished with  $\text{CeO}_2$  to a RMS roughness of  $0.25 \text{ nm}$  for an area of  $10 \times 10 \mu\text{m}^2$ . A hole of radius  $R = (0.531 \pm 0.010) \text{ mm}$  was drilled at their center to trigger the start of two symmetric fractures (see Fig. 3).

The measure of the crack opening profile is performed by means of monochromatic light reflection interferometry according to the sketch of Fig. 4. When observing the crack tip by AFM at the free surface of the sample, the crack front is vertical as in Fig. 3 b. In order to use the AFM setup to measure the crack opening displacement, the DCDC sample had to be placed with the fracture front lying horizontally. The white light source (illuminating vertically the

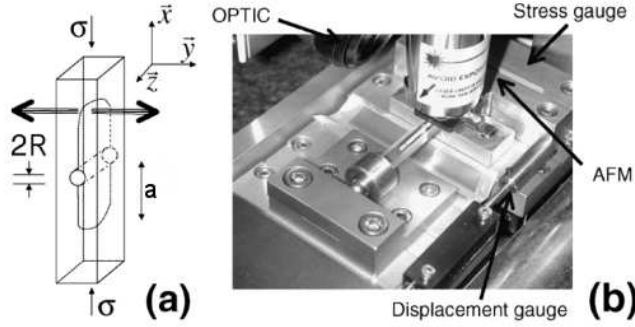


FIG. 3 – Experimental setup : (a) Sketch of the DCDC geometry ; (b) picture of the experiment

sample after passing through the optical axis on the CCD camera and being reflected by an inclined mirror in the AFM head) was substituted by a green laser source (wavelength  $\lambda = (532 \pm 1)$  nm) in order to provide an intense monochromatic light.

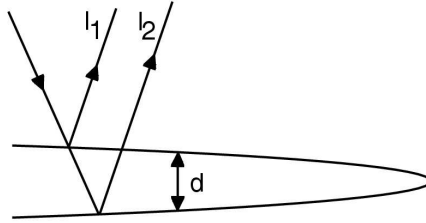


FIG. 4 – Sketch of the reflection interferometry technique at the crack tip of a glass sample. NB : exaggerated vertical scale for the crack opening and lateral scale for the reflected beams

When the monochromatic beam reaches the fracture plane in an orthogonal direction, it is splitted into two beams that are reflected by the two fracture surfaces and then collected back by the CCD camera. The path difference between the two beams is twice the distance between the two lips of the crack, *i.e.*  $\Delta = 2d = 4u_y(X)$  according to the notations used previously. The phase difference  $\delta$  is therefore given by

$$\delta = \pi + \frac{2\pi n}{\lambda} 4u_y(X) \quad (3)$$

where  $n$  is the refractive index of the fluid filling the gap in the fracture and the term  $\pi$  is a constant additive phase shift caused by the fact that both beams are normally reflected on symmetrically opposite interfaces (respectively glass/fluid and fluid/glass) [12].

The intensity  $I$  of the reflected light is given by :

$$I = I_1 + I_2 + 2(I_1 I_2)^{1/2} \cos(\delta) \simeq 4I_1 \cos^2\left(\frac{\delta}{2}\right) \quad (4)$$

where the approximation on the right stems from the fact that the two reflected beams have similar intensity. Since  $u_y(X)$  is a monotonically increasing function of  $X$ , the reflected intensity will develop into a series of fringes parallel to the crack front, each new one corresponding to an increase of the crack opening  $d = 2u_y(X)$  by a quantity  $\lambda/2$ . The term  $\pi$  in Eq. (3) implies the presence of an intensity minimum at  $X = 0$ . The first intensity maximum is obtained for  $2u_y(X_1) = \lambda/4$  and the position  $X_k$  of the  $k^{\text{th}}$  order fringe is given by the equation

$$2u_y(X_k) = \left(\frac{1}{2} + k\right) \frac{\lambda}{2}. \quad (5)$$

By measuring the position and order of the fringes along the whole crack, we obtain a series of discrete data points on the full crack opening profile as shown in Fig. 5.

In order to provide a better resolution, the fringe pattern along the 5 mm crack length is imaged with a series of 1 mm overlapping images. To insure that we preserve the right order and position of the fringes, the displacements of the load cell are measured by a heterodyne interferometer (Zygo) with 10 nm resolution. The incertitude on the position of each fringe was estimated depending on the quality of the local signal and fringe shape (the error bars are plotted in Fig. 5). A special attention must be paid to the first fringe, since the opening gradient is maximal in that region. However, in our operating conditions, the position of the first fringe is located to some hundreds of micrometers from the crack tip, making its measurement safe.

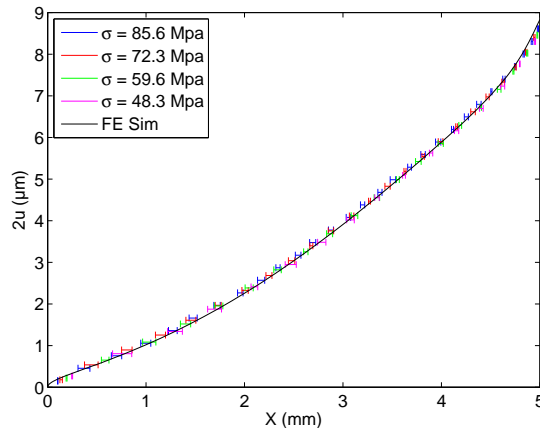


FIG. 5 – Comparison between the opening crack profile obtained by the four experiments (in color, with errorbars) at different loads (renormalized) and the results of the FE simulation for the same set of parameters

In order to verify the robustness of the method and the linearity of the loading configuration and sample, the measurement was repeated for four different loads ( $\sigma = 50, 62.5, 75$  and  $87.5$  MPa) and the opening profile was normalized to the reference load  $\sigma = 100$  MPa also used in the FE simulations according to linear elasticity. The four experimental series were realized in a time span of one hour in order to guarantee stable conditions ( $T = (21 \pm 1)^\circ$  C,  $RH = (35 \pm 5)$  %) and minimal crack propagation. Since the highest stress used in this experiment corresponds to  $K_I = 0.36$  MPa m<sup>1/2</sup>, the maximum crack propagation velocity is of the order of  $10^{-10}$  m s<sup>-1</sup>. The maximum crack advance in one hour can thus be estimated to  $0.4$   $\mu$ m, which is below the resolution of our optical microscope. The crack length can thus be considered as constant with the value  $a = (5.02 \pm 0.01)$  mm.

The results of Fig. 5 show an excellent agreement between the four measurements within the experimental errors. The agreement is also excellent when comparing the experimental measurements to the results of the FE simulation for the same set of parameters (represented by a black line on Fig. 5). We point out that the agreement with the FE simulations is also excellent in the diverging part near the central hole (corresponding to distances  $X \simeq a = 5$  mm from the crack tip). We should remind that the FE simulation is made in 2D under plane strain condition in order to represent the deformation field in the bulk of the DCDC specimen where the reflection interferometry is applied. When we refer to the crack length  $a$  in a 3D specimen, this should thus be measured in the center of the specimen.

Finally, due to the robustness of the crack opening profile shown in the previous section, the agreement between the FE simulation and the experimental measurements for a given sample geometry can be considered as representative for a broad set of geometrical parameters.

## 4 Mechanical effect of a liquid condensate inside the crack

In our recent works [13],[14],[4], we showed that the inner part of the crack cavity can be filled by a liquid condensation when the glass samples are submitted to moist atmosphere. The length of the condensate during slow crack propagation in silica glass samples was measured by means of in-situ AFM phase imaging techniques in controlled atmosphere. The condensate length was found to be always inferior to  $2$   $\mu$ m for crack in propagating conditions ( $K_I > 0.3$  MPa m<sup>1/2</sup>) and a relative humidity below 40%. Due to elevated confinement, the capillary condensation inside the crack tip is submitted to a very strong negative Laplace pressure  $\Delta P = \gamma/r_K$ , depending on the surface tension  $\gamma$  and the Kelvin radius  $r_K$  of the condensed liquid. We can reasonably limit the domain of variation of  $r_K$  between  $1$  nm (the typical curvature radius at the crack tip) and  $10$  nm ( $\sim Hc/2$ ). Using  $\gamma_{water} = 72$  mJ/m<sup>2</sup>, we obtain a negative pressure in the condensate between  $720$  and  $72$  bar, respectively. This

induces a reduction of the crack opening profile in the condensate region. We can estimate the distortion of the crack lips by using first order term of the equation (1) since the length of the observed condensate is far below  $\xi_1 = 20 \mu\text{m}$  and adding the action of the uniform attractive capillary forces inside the crack tip according to [10], [15].

That distortion is mainly localised along the condensate itself. For short condensates, the changes in the crack opening profile would hardly be detectable because the first maximum of intensity is beyond the region of influence of the condensate traction. This explains the good agreement observed in Fig. 5 where no internal forces were taken into account.

The mechanical effect of the the condensate could affect in a more significant way the determination of the critical condensation distance that we made in our AFM experiments [4]. In this previous work, we have measured the length  $L_{cond}$  of the liquid condensate as a function of the stress intensity factor  $K_I$  for three different values of the relative humidity. We have then confronted these results to two models relating  $L_{cond}$  and  $K_I$ , the first one with the hypothesis that the liquid were evaporating/condensing too slowly to affect the condensate volume and the second one that it was quick enough to reach equilibrium. The three experimental series of data  $K_I - L_{cond}$  have clearly shown that the equilibrium was reached and that the critical condensation distance  $H_c$  was thus possible to be determined. This determination was yet made without taking into account the potential mechanical effect of the condensate that we assumed to be small. Taking it into account, we can now express more generally the critical condensation distance for length  $L_{cond} \ll a$  by :

$$H_c(L_{cond}, K_I, \Delta P) = 2 \frac{K_I}{E'} \sqrt{\frac{8L_{cond}}{\pi}} - \frac{4\Delta P}{E'} \left( \frac{4L_{cond}}{\pi} + \frac{a}{\sqrt{2\pi L_{cond}}} \log \left( \frac{a - L_{cond}}{L_{cond}} \right) \right) \quad (6)$$

Our previous determination corresponded to  $\Delta P = 0$ . The value of the internal pressure  $\Delta P$  is not well known at present due to the difficulty of accessing the details of the chemistry of the nanoscale condensation. However, equation (6) can be used to estimate some extreme effects. Fig. 6 shows the data corresponding to the lower value of the relative humidity which is the one that implies the highest  $\Delta P$ . The two lines represent the best fits corresponding to the two extreme cases. In the case of  $\Delta P = 72$  bar, the effect on  $H_c$  is completely negligible, the estimated critical distance is  $H_c = 16$  nm as for the case with  $\Delta P = 0$  bar. In the worst case scenario of  $\Delta P = 720$  bar the estimates of  $H_c$  is reduced to the value  $H_c = 13.7$  nm. In both cases, the model remains relevant to fit the data. Taking into account the capillary forces does not infrim the conclusion reached in our previous article [4]. The effect on the determination of the condensation critical distance  $H_c$  would be almost of the order of 14% in the worst case scenario.

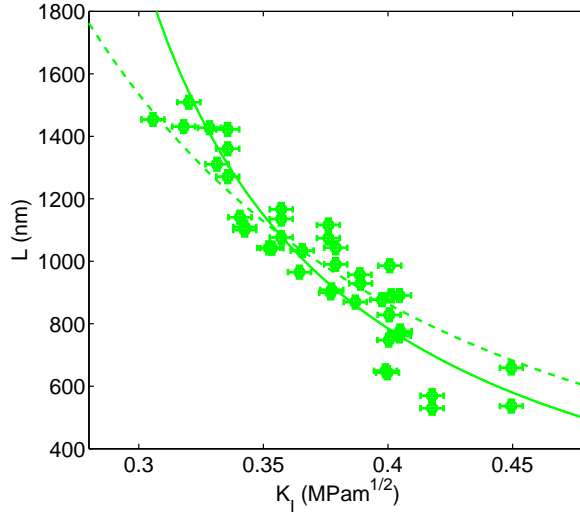


FIG. 6 – Condensation length  $L_{cond}$  versus  $K_I$  at  $RH = 6\%$  [4]. Estimation of the effect of the capillary forces on the determination of the critical distance  $H_c$  for  $K_I - L_{cond}$  curves. The curves represent the best fit for each condition (dashed :  $\Delta P = 72$  bar, plain :  $\Delta P = 720$  bar).

## 5 Conclusion

This work reports a combined theoretical and experimental study of the crack opening profile in DCDC specimens of linear elastic materials. It has been shown how a fifth order Williams expansion series can be used to describe very accurately the crack opening profile over a conveniently large domain near the crack tip. Finite element simulations have allowed to express the crack opening profile in a simple form as a function of the geometrical parameters of the specimen. The ranges of validity of these analytical expressions and more specifically of the Williams development at various orders are calculated. Moreover, the simulated profiles were successfully tested against an accurate experimental measurement performed by means of monochromatic light interference experiments. The implications of this analysis on the interpretation of recent important experimental measurements by AFM of the submicrometric capillary condensation at crack tips in silica glass are discussed. The crack opening at the end of the condensed region was expressed by a simple analytical equation. The relation between the external stress intensity factor and the equilibrium condensation length could then be modeled. The mechanical effect induced by capillary forces was shown to have a worst case effect of 14% on the determination of the critical distance  $H_c$ .

Acknowledgements - We wish to thank C. Marlière for initial developments of the fracture experiment and C. Blanc for his help in the setup of the interferometric technique. This work was supported by the ANR grant CORCOSIL (BLAN07-3-196000).

## Références

- [1] C. Janssen, Specimen for fracture mechanics studies on glass. In : C.B. Biezeno, J.M. Burgers (Eds.), Proceedings of the 10th International Congress on glass in Tokyo, 1974, pp 10.23–10.30
- [2] F. Célarié, S. Prades, D. Bonamy, L. Ferrero, E. Bouchaud, C. Guillot, C. Marlière, Glass breaks like metal but at the nanometer scale, *Phys Rev Lett* (2003) 90 :075504
- [3] D. Bonamy, S. Prades, L. Ponson, D. Dalmas, C.L. Rountree, E. Bouchaud, C. Guillot, Experimental investigation of damage and fracture in glassy materials at the nanometer scale, *Int J Prod Tech*(2006) 26 :339–353
- [4] A. Grimaldi, M. George, G. Pallares, C. Malière, M. Ciccotti, The crack tip : a nanolab for studying confined liquids, *Phys Rev Lett* (2008) 100 :165505
- [5] T. Fett, G. Rizzi, D. Creek, S. Wagner, J.P. Guin, J.M. López-Cepero, S.M. Wiederhorn, Finite element analysis of a crack tip in silicate glass : No evidence for a plastic zone, *Phys Rev B* (2008) 77 :174110
- [6] T.A. Plaisted, A.V. Amirkhizi, S. Nemat-Nasser, Compression-induced axial crack propagation in DCDC polymer samples : experiments and modelling, *Int J Fract* (2006) 141 :447–457
- [7] T.J. Lardner, S. Charkravathy, J.D. Quinn, J.E. Ritter, Further analysis of the DCDC specimen with an offset hole, *Int J Fract* (2001) 109 :227–237
- [8] T. Fett, G. Rizzi, D. Munz, T-stress solution for DCDC specimens, *Eng Fract Mech* (2005) 72 :145–149
- [9] M.L. Williams, On the stress distribution at the base of a stationary crack, *ASME J Appl Mech* (1957) 24 :109–114
- [10] B. Lawn, *Fracture of Brittle Solids*, 2nd ed. Cambridge University Press, Cambridge, 1993
- [11] F. Célarié, Ph.D. thesis, Université Montpellier 2, France, 2004
- [12] M. Born, E. Wolf, *Principles of optics : electromagnetic theory of propagation, interference and diffraction of light*, 7th ed. Cambridge University Press, Cambridge, 1999
- [13] L. Wondraczek, A. Dittmar, C. Oelgardt, F. Célarié, M. Ciccotti, C. Marlière, Real-time observation of non-equilibrium liquid condensate confined at tensile crack tips in oxide glasses, *J Am Ceram Soc* (2006) 89 :746–749
- [14] M. Ciccotti, M. George, V. Ranieri, L. Wondraczek, C. Marlière, Dynamic condensation of water at crack tips in fused silica glass, *J Non-Crist Solids* (2008) 354 :564–568

- [15] D. Maugis, Contact, Adhesion and Rupture of Elastic Solids, 2nd ed. Springer-Verlag, Heidelberg, 1999